XVIII. DETECTION AND ESTIMATION THEORY*

Academic Research Staff

Prof. H. L. Van Trees
Prof. A. B. Baggeroer

Graduate Students

J. P. Albuquerque
L. S. Metzger
J. M. F. Moura
S. Orphanoudakis
S. A. Parl
L. C. Pusey
K. B. Theriault

RESEARCH OBJECTIVES AND SUMMARY OF RESEARCH

The research of this group is focused on the theory of detection and estimation and its application to development of effective signal-processing methods. Specific areas of current interest include nonlinear estimation theory, array processing, detection theory for random processes, and signal processing for oceanographic research.

1. Nonlinear Estimation Theory and Array Processing

Array receiver structures for tracking the motion of targets using only passive signals have been developed. The "bearings only" problem has been investigated in a state-variable context. The effects of target motion on the temporal structure of signals, e.g., Doppler effects, have been incorporated, and lead to a receiver structure that is similar to a phase-locked loop coupled to a split-beam tracker. Spatial effects of angle of arrival and wavefront curvature have been investigated. A summary of a Master's thesis by J. M. F. Moura, to be submitted to the Department of Electrical Engineering in February 1973, appears in Section XVIII-A. L. S. Metzger and S. Orphanoudakis are also involved in this research.

H. L. Van Trees, A. B. Baggeroer

2. Theory of Random-Process Detection and Modeling

In many applications of random-process detection, a stochastic model constructed from an observation of a segment of noisy sample function is wanted. Many methods have been developed to meet this problem. One issue of particular importance is the sensitivity of these methods and the degree to which different stochastic models can be separated or detected. Work directed at quantifying this sensitivity is being developed by J. P. Albuquerque.

The theory of estimating temporal random processes has been studied extensively. In contrast, study of the structure of spatial random process estimators is just starting. S. A. Parl is formulating the problem of estimating random processes generated by a propagating dynamical structure. This work involves aspects of distributed random processes, and he is applying it to the example of estimating oceanic internal waves.

A. B. Baggeroer

*This work is supported by the Joint Services Electronics Programs (U.S. Army, U.S. Navy, U.S. Air Force) under Contract DAAB07-71-C-0300, and the National Science Foundation (Grant GX-36331).

3. Application of Detection and Estimation Methods to the East Atlantic Continental Margin Program

This work is being done in cooperation with scientists from the Geology and Geophysics Department at Woods Hole Oceanographic Institution. It is directed toward developing models and algorithms for shipboard processing for the signals that are employed in continuous seismic profiling of the sea floor. During a cruise to the West Coast of Africa last year, a parameter-estimation model for in situ removal of water column multiples was developed and reported in Quarterly Progress Report No. 107 (pp. 95-101). We are now developing these methods further using the models of spread channel from communication theory. We are also studying state-variable models for horizon tracking, parameter estimation for matched filtering of seismic source signals, and velocity estimation. Experiments resulting from these studies will be conducted at sea during the forthcoming National Science Foundation International Decade of Ocean Exploration cruise to the East Atlantic Continental Margin off Northern Africa.

A. B. Baggeroer

A. AN INTEGRATED APPROACH TO THE ESTIMATION OF THE DYNAMICS OF A MOVING SOURCE BY A PASSIVE OBSERVER

Joint Services Electronics Programs (Contract DAAB07-71-C-0300)

J. M. F. Moura

1. Introduction

We shall consider an integrated model[1] for the estimation of the dynamics of a moving source (MS) from observed acoustical data by a passive linear array.

The changes induced by the source dynamics in the spatial and temporal structure of the emitted narrow-band signal are processed by a spatially and temporally coupled receiver that simultaneously estimates the range and bearing and their time derivatives modeled as finite-state dimensional stochastic processes.

The MS dynamics is studied in two frameworks, rectangular and polar, both of which lead to a nonlinear estimation problem. After linearizing the problem, the extended Kalman filter and the maximum a posteriori filter (discrete version) are applied. Monte Carlo simulation studies have shown that regions of convergence for the geometry, the signal-to-noise ratio, and the driving noise power level can be found for all processors. In order to prevent numerical divergence from the polar frame that would result from an ill-conditioned error-covariance matrix, a square-root filter was implemented. The necessary a priori information to start the filters was obtained by means of a maximum-likelihood algorithm followed by a triangularization procedure.

2. Model

We describe the stochastic dynamical system modeling the MS and the model for the received signal. For simplicity, we assume a stationary observer (discrete linear

array), planar geometry, and a far-field hypothesis.

We shall consider two coordinate systems, the polar and rectangular frames

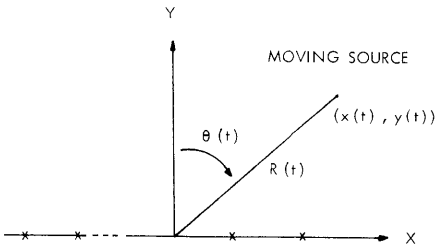

Fig. XVIII-1. Planar geometry.

shown in Fig. XVIII-1, with the usual relations

$$R(t) = \sqrt{x^2(t) + y^2(t)} \tag{1}$$

$$\theta(t) = \tan^{-1}(x(t)/y(t)).$$

The linear observer has N sensors at locations $p_1, \ldots p_N$, along the x axis.

a. Received Signal

The MS generates a narrow-band signal modeled as

$$h(t) = \sqrt{2P} \sin w_c t, \tag{2}$$

where P is the transmitted power.

At the reference sensor a delayed version of h(t) is received, corrupted by additive noise

$$\begin{aligned} r_o(t) &= h_o(t) + w_o(t) \\ &= h(t-\tau_o(t)) + w_o(t), \end{aligned} \tag{3}$$

where $\tau_o(t)$ is the travel time of the wavefront from the MS to the reference element, which is given by

$$\tau_o(t) = \frac{R(t-\tau_o(t))}{c}, \tag{4}$$

and c is the medium propagation velocity.

At the i^{th} sensor

$$\begin{aligned} r_i(t) &= h_i(t) + w_i(t) \\ &= h_o(t+\tau_i(t)) + w_i(t), \end{aligned} \tag{5}$$

where the relative delay $\tau_i(t)$ to the reference element is

$$\tau_i(t) = \frac{\sin\theta(t-\tau_o(t+\tau_i(t))+\tau_i(t))}{c}\, p_i. \tag{6}$$

Expressions 4 and 6 are memory functions of the dynamics, which can be approximated by exploiting the narrow-band assumption on the signal by means of truncated Taylor series expansions,[2] by no-memory functions leading to

$$r_i(t) = \sqrt{2P}\, \sin w_c\left(t - \frac{R(t)}{c} + \frac{p_i}{c}\sin\theta(t)\right) + w_i(t) \tag{7}$$

for $i = 1, \ldots, N$.

The additive noises $w_i(t)$ are assumed to be sample functions of uncorrelated zero-mean white Gaussian noises with spectral heights $N_o/2$.

b. Dynamical System

Newton's law gives the dynamical system equation. Modeling the MS acceleration components by sample functions of a (mathematical) white-noise process yields in rectangular coordinates

$$\begin{aligned}\underline{\dot{x}}(t) &= \underline{F}\,\underline{x}(t) + \underline{G}\,\underline{u}(t)\\ &= \begin{bmatrix}0&1&0&0\\0&0&0&0\\0&0&0&1\\0&0&0&0\end{bmatrix}\begin{bmatrix}x(t)\\\dot{x}(t)\\y(t)\\\dot{y}(t)\end{bmatrix} + \begin{bmatrix}0&0\\1&0\\0&0\\0&1\end{bmatrix}\begin{bmatrix}u_x(t)\\u_y(t)\end{bmatrix}\end{aligned} \tag{8}$$

with $\underline{x}(0) = \underline{x}_o$.

By a simple transformation of coordinates, from (8), we obtain in polar coordinates

$$\begin{aligned}\underline{\dot{x}}(t) &= \underline{f}(\underline{x}(t)) + \underline{g}(\underline{x}(t))\,\underline{u}(t)\\ \begin{bmatrix}\dot{R}(t)\\\ddot{R}(t)\\\dot{\theta}(t)\\\ddot{\theta}(t)\end{bmatrix} &= \begin{bmatrix}\dot{R}(t)\\R(t)\,\dot{\theta}(t)^2\\\dot{\theta}(t)\\-2\dot{R}(t)\,\dot{\theta}(t)/R(t)\end{bmatrix} + \begin{bmatrix}0&0\\\sin\theta(t)&\cos(t)\\0&0\\\cos\theta(t)/R(t)&-\sin\theta(t)/R(t)\end{bmatrix}\begin{bmatrix}u_x(t)\\u_y(t)\end{bmatrix}\end{aligned} \tag{9}$$

with $\underline{x}(0) = \underline{x}_o$.

The stochastic interpretation of Eq. 8 does not offer any ambiguity. With the polar system it can be shown[2] that either the Ito or the Stratonovitch integral leads to the same model, since the Wong-Zakai correction terms[3] are zero for the particular $\underline{g}(\cdot)$ matrix in Eq. 9.

We observe that in rectangular coordinates the system is linear. The MS parameter range, bearing, and respective rates are given by a nonlinear transformation of the state variables. With the polar frame we choose as state variables the MS parameters, but the dynamical system becomes nonlinear.

The driving processes $u_x(t)$ and $u_y(t)$ are assumed to be zero-mean white Gaussian noise with spectral heights Q, independent of the $w_i(t)$ noise and of the initial condition $\underline{x}_o$ which is modeled as a random variable of mean $\hat{\underline{x}}_o$ and covariance matrix $\underline{P}_o$.

3. Nonlinear Estimation Problem

For simplicity, we worked with the sampled version of this continuous time estimation problem. Only filters with a first-order approximation are considered.[2] In particular, we implemented the extended Kalman filter and the maximum a posteriori filter (MAP).[4]

With the discrete extended Kalman filter we used the following format.

(i) Measurement Update Equations (Correction)

The estimator equation is

$$\hat{\underline{x}}_k = \bar{\underline{x}}_k + \underline{P}_k \underline{H}_k^T \underline{R}_k^{-1} (\underline{r}_k - \underline{h}(\bar{\underline{x}}_k, k)) \tag{10}$$

$$\hat{\underline{x}}_o = E\underline{x}_o.$$

The covariance propagation equation is

$$\underline{P}_k = \left[\underline{M}_k^{-1} + \underline{H}_k^T \underline{R}_k^{-1} \underline{H}_k \right]^{-1}, \tag{11}$$

with $\underline{P}_o$ = covariant $(\underline{x}_o, \underline{x}_o)$.

(ii) Time Update Equations (Prediction)

The estimator equation is

$$\bar{\underline{x}}_{k+1} = \underline{f}(\hat{\underline{x}}_k) + \underline{g}(\hat{\underline{x}}_k)\, \bar{\underline{u}}_k. \tag{12}$$

The covariance propagation equation is

$$\underline{M}_{k+1} = \frac{\partial \underline{f}}{\partial \hat{\underline{x}}_k} \underline{P}_k \left(\frac{\partial \underline{f}}{\partial \hat{\underline{x}}_k} \right)^T + \underline{g}(\hat{\underline{x}}_k) \underline{Q} \underline{g}^T(\hat{\underline{x}}_k). \tag{13}$$

The MAP filter is similar to the extended Kalman filter. The principal difference is in the measurement update equation which, instead of (11), becomes

$$\underline{P}_k = \left[\underline{M}_k^{-1} - \frac{\partial}{\partial \bar{\underline{x}}_k} \left\{ \underline{H}_k^T \underline{R}_k^{-1} (\underline{r}_k - \underline{h}(\bar{\underline{x}}_k, k)) \right\} \right]^{-1}. \tag{14}$$

With

$$- \frac{\partial}{\partial \bar{\underline{x}}_k} \left[\underline{H}_k^T \underline{R}_k^{-1} (\underline{r}_k - \underline{h}(\bar{\underline{x}}_k, k)) \right] \geq 0, \tag{15}$$

a matrix $\hat{\underline{H}}_k$ can be found such that

$$\hat{\underline{H}}_k \underline{R}_k^{-1} \hat{\underline{H}}_k = - \frac{\partial}{\partial \bar{\underline{x}}_k} \left[\underline{H}_k^T \underline{R}_k^{-1} (\underline{r}_k - \underline{h}(\bar{\underline{x}}_k, k)) \right], \tag{16}$$

and so we can formally reduce Eq. 14 to Eq. 11.

Given the observations at time k, the error-covariance matrix $\underline{P}_k$ as computed by using the MAP has a random component that becomes more important as the signal-to-noise ratio decreases and may cause $\underline{P}_k$ to become indefinite and the filter to diverge.

In the polar framework, because of the presence in the state vector of the range and the bearing rate, the filtering problem is computationally ill-conditioned; that is, the condition number

$$\mu(\underline{P}) = \frac{\text{maximum eigenvalue of } \underline{P}}{\text{minimum eigenvalue of } \underline{P}}$$

of the error covariance matrix is very large. This leads to numerical divergence problems. These difficulties were overcome[2] by implementing a square-root algorithm (e.g., Kaminski et al.[5]). We modified Potter's method[6] by using an argument of Andrews[7] to get a computable solution for the case wherein the number of observations is much larger than the dimension of the state vector.

4. Mathematical Analysis of the Receivers

We shall now discuss the filter for the polar frame. Other configurations, and additional details have been given elsewhere.[2]

a. Estimator Equations

Figure XVIII-2 is a block diagram for the estimator equations. Essentially, the filter combines the innovation processes

$$\underline{r}(t) - \underline{h}(\underline{\bar{x}}(t))$$

to form a conventional delay and sum array beam Z1 and a "difference" beam Z3. The farthest right side of Fig. XVIII-2 shows the combining matrix operation $\underline{P}$ followed by the conventional receiver's copy of the dynamical system.

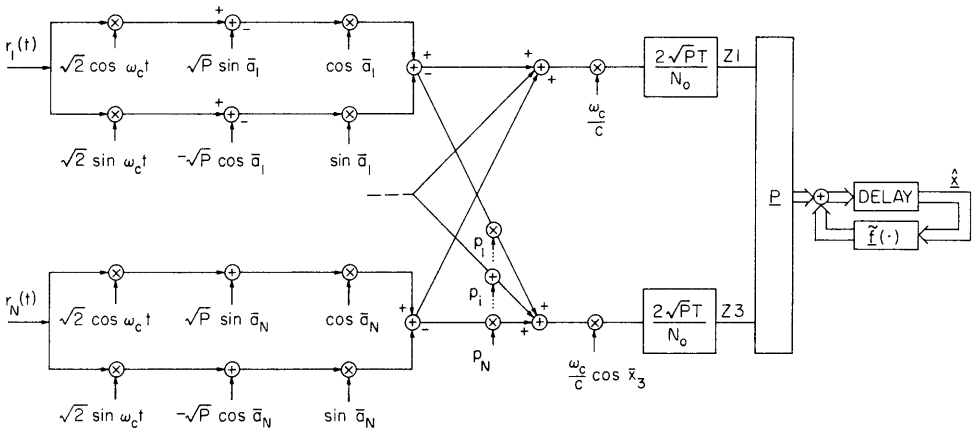

Fig. XVIII-2. Estimator processor: polar system.

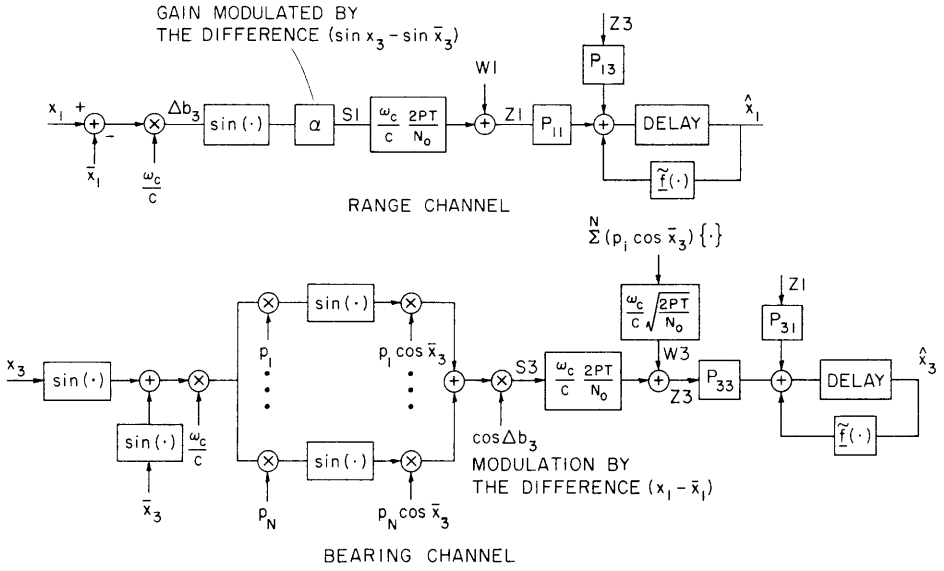

Fig. XVIII-3. Range and bearing channel in polar coordinates.

Figure XVIII-2 can be rearranged in the form of Fig. XVIII-3 which shows the decoupled range and bearing channels.

Figure XVIII-4 illustrates the estimator channel for the four-state variable. The coupling effect between the channels is introduced mainly by the crosscovariances.

If

$$P_{11} \gg P_{13}$$
$$P_{33} \gg P_{13}, \tag{17}$$

the range channel and the bearing channel perform as phase-locked loops to track the waveforms

$$\phi_1(t) = \frac{w_c}{c} R(t) \tag{18}$$

and

$$\phi_2(t) = \frac{w_c}{c} \sin \theta(t). \tag{19}$$

The filter can estimate the range and bearing rates through the modulation of the received waveforms induced by the MS. At each rate channel both beams Z1 and Z3

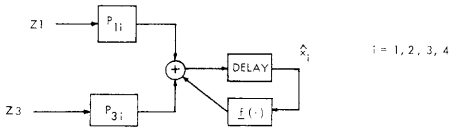

Fig. XVIII-4. Estimator channel.

are present; the weights are the respective error crosscovariances P_{1j} and P_{3j}, $j = 2, 4$.

Because the filter behaves like a phase-locked loop, it exhibits a primary lock-in region of an interval of one wavelength centered on the true range.

We observe that the dependence of the MAP covariance equation on the actual errors of the estimates shows that the propagated covariances, and consequently the Kalman gain, will tend to follow the actual errors. Physically, the filter bandwidth is directly modeled by the errors in the estimates.

b. Covariance Equation

Since the term $\underline{B} = \underline{H}^T \underline{R}^{-1} \underline{H}$ is the Fisher information matrix, the error covariances propagated by the Kalman filter are bounded above by the Cramer-Rao bounds

for the nonrandom unknown parameter case. This reflects the incorporation of the a priori information when modeling the processes $\theta(t)$ and $R(t)$ generated by a finite-dimensional dynamical system. For this problem we have

$$P_{RR} < B_{11} = \frac{1}{\frac{2PT}{N_o}\left(\frac{w_c}{c}\right)^2 N} \tag{20}$$

$$P_{\theta\theta} < B_{33} = \frac{1}{\frac{2PT}{N_o}\left(\frac{w_c}{c}\right)^2 \cos^2\theta \, \Sigma \, p_i^2}. \tag{21}$$

5. Monte Carlo Simulation

The receiver structures were simulated for several geometric configurations and different sets of parameters and initial conditions on a digital computer.

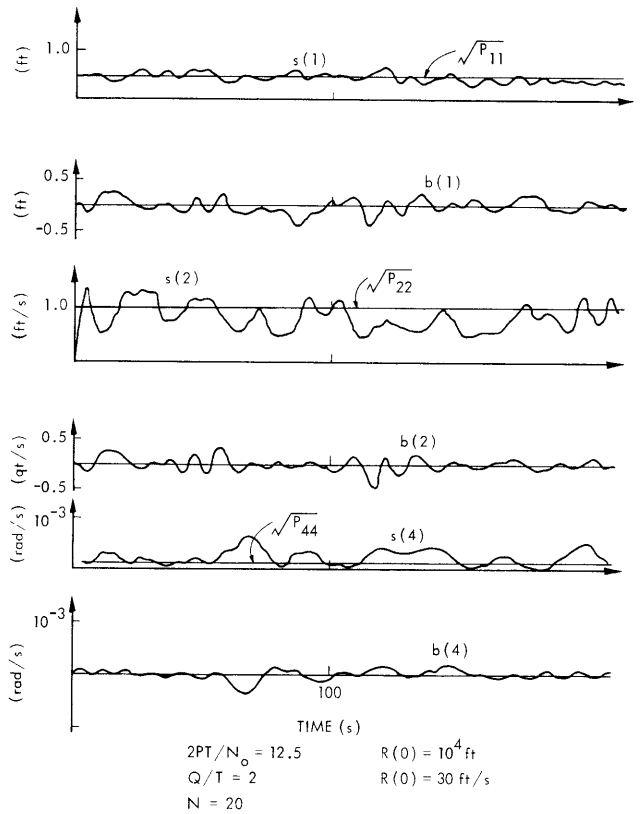

Fig. XVIII-5. Typical statistical history for 4 linearized filters.

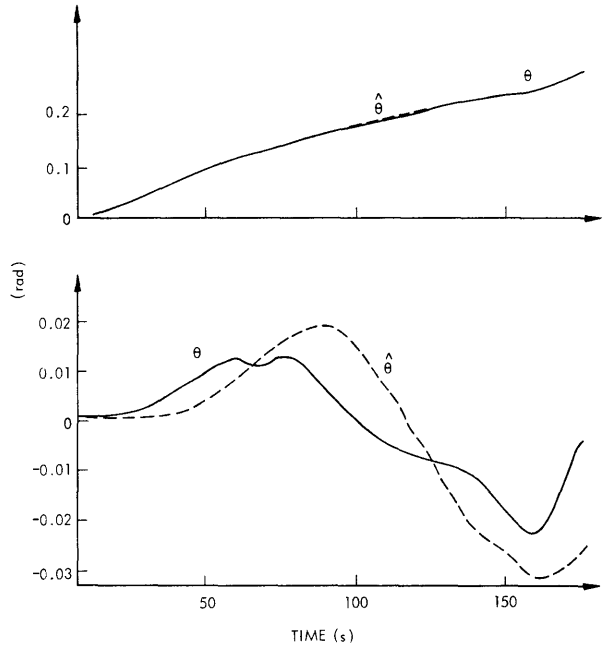

Fig. XVIII-6. Bearing-angle history for two different initial bearing rates (SQRT, Polar, EKF).

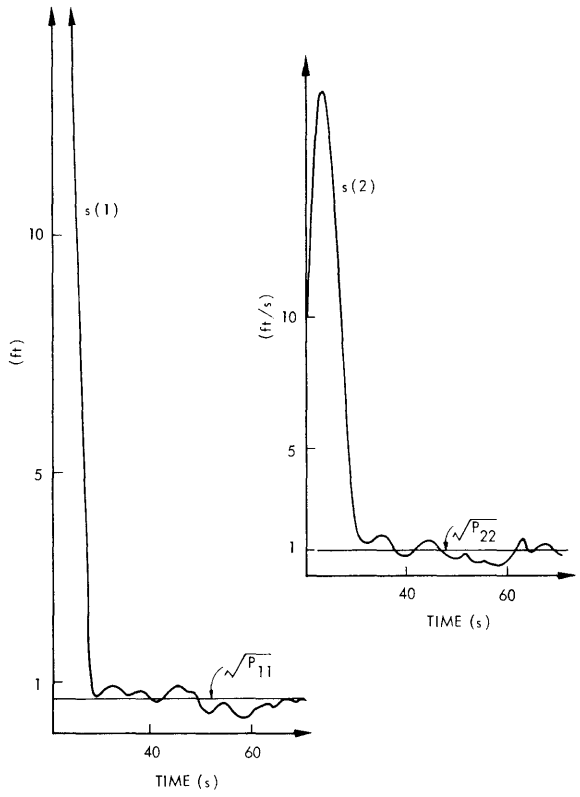

Fig. XVIII-7. Study of an initial error of range and range-rate estimates on the standard deviations (Polar, EKF, SQRT).

The performance was measured by the bias

$$\underline{b}(i) = \begin{bmatrix} b_1(i) \\ \cdots \\ b_4(i) \end{bmatrix} \tag{22}$$

and the standard deviation

$$\underline{s}(i) = \begin{bmatrix} s_1(i) \\ \cdots \\ s_4(i) \end{bmatrix}. \tag{23}$$

We fixed the wavelength at $\lambda = 50$ ft. In Figs. XVIII-5 and XVIII-6 the typical behavior of the 4 filters is summarized.

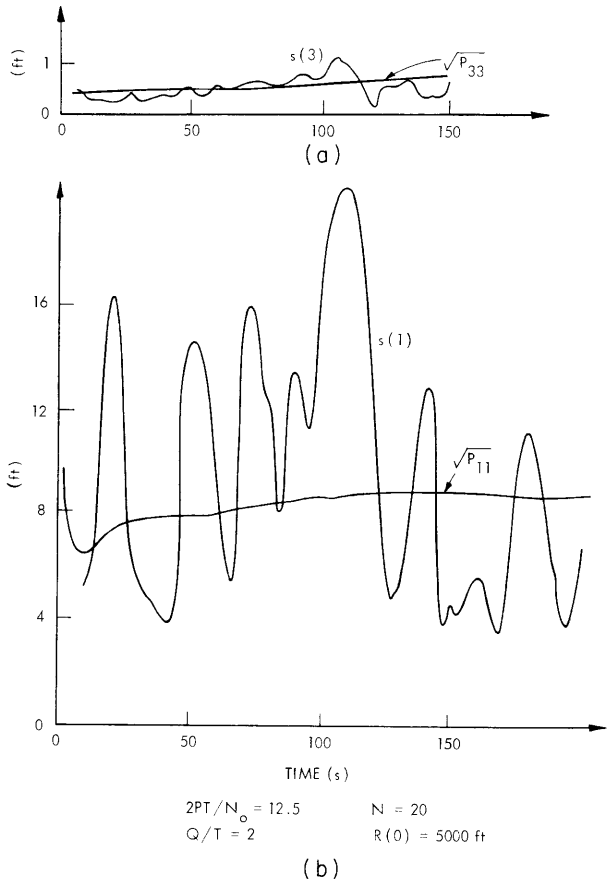

Fig. XVIII-8. History of (a) Y-channel and (b) X-channel for EKF rectangular-coordinate receiver.

The 4 filters work in a linear region in the sense that

$$s_j \rightarrow \sqrt{P_{jj}} \qquad j = 1, \ldots, 4 \tag{24}$$

and they give unbiased estimates.

Figure XVIII-7 considers a nonzero initial error on the range and range rate for the polar configuration. As long as the range is inside the primary lock-in region, the filters converge to the right range value. The filters are not very sensitive to the initial error in the range rate.

Figure XVIII-8 gives a comparison of the X- and Y-channels in rectangular coordinates for a broadside geometry. We observe that the Y-channel has a behavior similar to the range channel of the polar frame.

If for the rectangular system we derive bounds similar to Eqs. 17 and 18 (or equivalently compute the Cramer-Rao bounds for the X and Y coordinates which are now considered nonrandom unknown parameters), we would find that for a broadside configuration the bound for the X-channel is much larger than that for the Y-channel; this is shown in the experimental results given in Fig. XVIII-8.

Figure XVIII-9 shows the typical behavior of the EKF and MAP filters when we vary Q/T and $2PT/N_o$. As we increment the driving noise level, the steady-state error

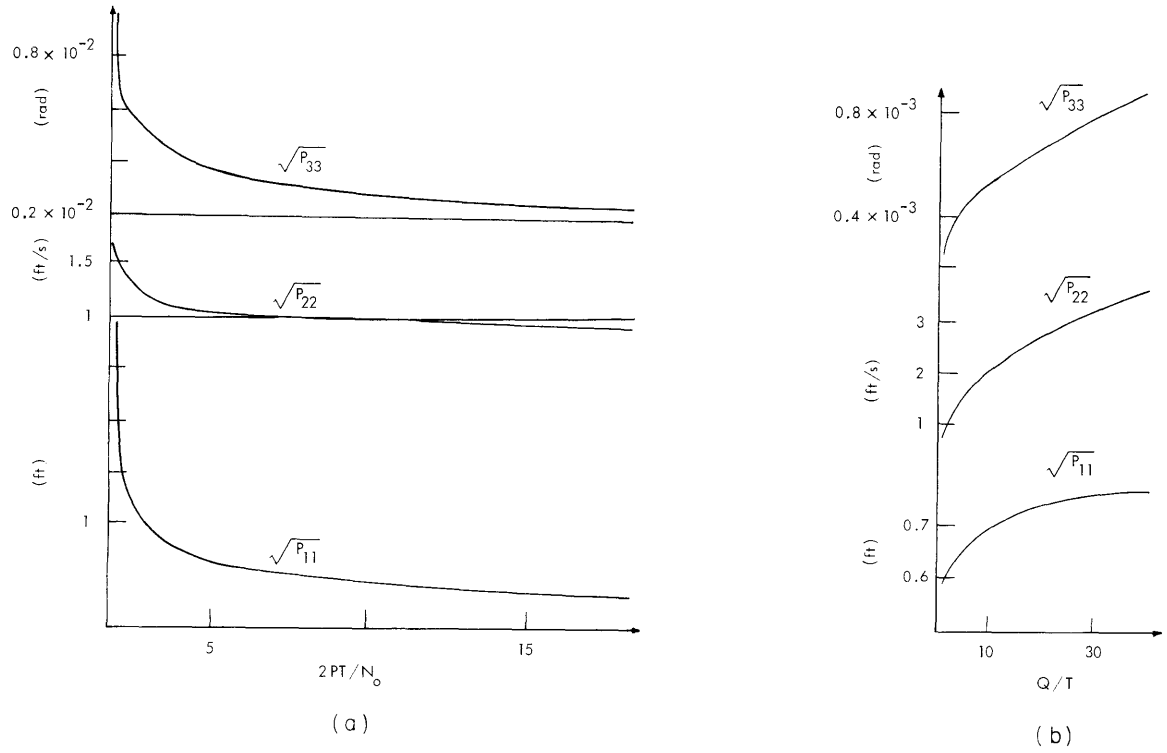

Fig. XVIII-9. EKF, Polar, SQRT performance. (a) Effect of signal-to-noise ratio. (b) Effect of Q.

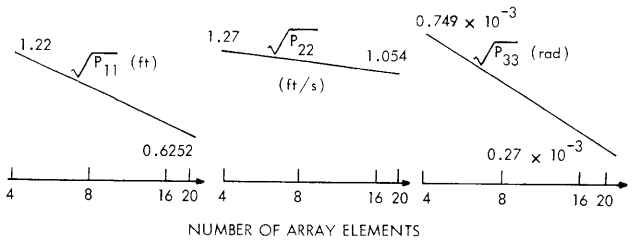

Fig. XVIII-10. Effect of array length on filter performance (Polar, EKF, SQRT).

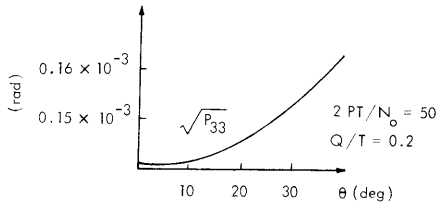

Fig. XVIII-11. Effect of range on bearing-channel performance (EKF, Polar, SQRT).

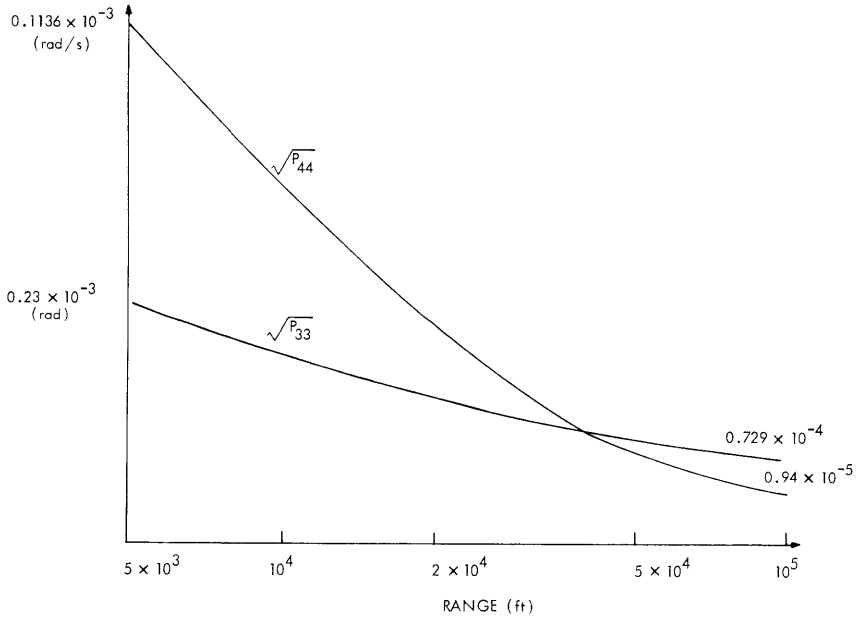

Fig. XVIII-12. Effect of bearing on bearing-channel performance (EKF, Polar, SQRT).

covariances increase, and so the Kalman gain increases. This means that a greater bandwidth is necessary for the filter to follow the larger source dynamics.

The filters exhibited a sharp threshold for the signal-to-noise ratio which is in the neighborhood of 1. In several runs the MAP filter diverged even for values of $2PT/N_o$ above threshold. This divergence was traced to the fact that the error-covariance matrix lost its positive semidefinite character. The square-root algorithm cannot obviate this.

Figures XVIII-10 through XVIII-12 show the effects of array length and tracking geometry on performance.

6. Conclusion

These simulation studies have shown that the modulation induced on the temporal and spatial structure of the signal by a moving source (MS) permits simultaneous estimation of MS dynamical parameters.

The (computationally) ill-conditioned polar-frame estimation problem can be solved by the square-root algorithm. All filters examined showed a sharp threshold on the signal-to-noise ratio and the performance of the filters depended also on the driving noise power level, array length, and tracking geometry.

Because of the nonlinear character of the estimation problem and the fact that the filter behaves like a phase-locked loop, some a priori information is needed in order to start the filters. By remodeling the received signal and considering the bearing as a nonrandom unknown quantity, provided we use a sufficiently large array, we are able[2] to solve for the starting information by means of a maximum-likelihood estimation algorithm (composite hypothesis test) followed by a triangularization procedure in which the curvature of the incoming wavefronts is considered.

References

1. H. L. Van Trees, Memorandum, Research Laboratory of Electronics, M.I.T., October 1971 (unpublished).
2. J. M. F. Moura, S.M. Thesis, Department of Electrical Engineering, M.I.T. (to be submitted February 1973).
3. A. H. Jazwinski, Stochastic Processes and Filtering Theory (Academic Press, Inc., New York, 1970).
4. A. P. Sage and J. L. Melsa, Estimation Theory with Applications to Communications and Control (McGraw-Hill Book Company, New York, 1972).
5. P. G. Kaminski, A. E. Bryson, and S. F. Schmidt, "Discrete Square Root Filtering: A Survey of Current Techniques," IEEE Trans., Vol. AC-16, No. 6, pp. 727-736, December 1971.
6. R. H. Battin, Astronautical Guidance (McGraw-Hill Book Company, New York, 1964).
7. A. Andrews, "A Square Root Formulation of the Kalman Covariance Equation," AIAA J. 6, 1165-1166 (1968).